JOURNAL OF AGRICULTURAL AND FOOD CHEMISTRY



# Infrared Imaging of Sunflower and Maize Root Anatomy

KENNETH M. DOKKEN† AND LAWRENCE C. DAVIS*

Department of Biochemistry, Kansas State University, 141 Chalmers Hall, Manhattan, Kansas 66506

Synchrotron radiation infrared microspectroscopy (SR−IMS) permits the direct analysis of plant cell-wall architecture at the cellular level *in situ*, combining spatially localized information and chemical information from IR absorbances to produce a chemical map that can be linked to a particular morphology or functional group. This study demonstrated the use of SR−IMS to probe biopolymers, such as cellulose, lignin, and proteins, in the root tissue of hydroponically grown sunflower and maize plants. Principal components analysis (PCA) was employed to reveal the major spectral variance between maize and sunflower plant tissues. The use of PCA showed distinct separation of maize and sunflower samples using the IR spectra of the epidermis and xylem. The infrared band at 1635 $cm^{-1}$, representing hydrocinnamic acid in (H type) lignin, provided a conclusive means of distinguishing between maize and sunflower plant tissues.

**KEYWORDS: Infrared imaging; FTIR microspectroscopy; synchrotron radiation; plant tissue; principal components analysis**

## INTRODUCTION

Over the past decade, infrared microspectroscopy (IMS) has emerged as a tool to study plant growth and development at the molecular level. A fair amount of work has been published showing the ability of IMS to study plant cell wall architecture (*1–4*). However, this work focused primarily on cell-wall extracts and very little on whole plant tissue. One major disadvantage for studying extracted cell-wall material is the loss of the spatial distribution of microstructures in the plant tissue. The low source brightness of globar sources from benchtop instruments along with conventional single detectors gives spatial resolution limited by signal-to-noise considerations. More recently, the study of whole plant tissue using IMS became more feasible because of the coupling of IMS to a synchrotron source. The high energy of synchrotron radiation (SR) has provided dramatic improvements for studying plant samples. The small effective source size and high brightness of the synchrotron beam allows for the study of samples with small areas with spatial resolution to the diffraction limit of 5–15 $\mu$m. However, the use of SR−IMS to study plant structures is still in its infancy.

There are a limited number of research groups that use SR−IMS to study plant microstructures. Most of these studies have focused on feed (seed) tissues, such as wheat (*5–9*), corn (*8, 10, 11*), oat (*7–9*), barley (*8, 9, 12–14*), and canola seeds (*8, 15*). Fewer than 10 reports have focused on whole plant tissue (*7, 16–19*). The lack of research on whole plant tissue may stem from the complexity of the biopolymers in plant tissues, such as cellulose and lignin, compared to seed tissue composed primarily of a starchy matrix containing lipids and proteins. The less complex structure of seed tissues makes it easier to resolve the spatial distribution of infrared functional groups with respect to seed microstructures.

This paper will focus on the ability of SR−IMS to probe complex microstructures and biopolymers in the root tissue of sunflower and maize plants. The intention will be to perform an "infrared dissection", from the root cap to 1 cm up the root, to observe the spectral differences between different tissues types, such as xylem and epidermis. The potential of SR−IMS to differentiate between two different plant species, using maize and sunflower as the representative organisms, will also be assessed. Very few works have looked at the spectral differences between monocots and dicots. Sene et al. (*20*) and McCann et al. (*21*) used IMS to study cell-wall material of several different monocots and dicots and noted some broad differences in the spectral regions associated with pectins and proteins. However, the high complexity of plant cell walls and natural variation between plants of the same group has made this task difficult. Principal components analysis (PCA) was employed to further uncover spectral differences between the two plant types.

## MATERIALS AND METHODS

**Materials.** Commercial oilseed-type sunflower seeds and Pioneer maize seeds (hybrid 32M38) were germinated by either the vermiculite method, as previously reported by Castro et al. (*22*) or the Petri-dish method. All seeds were soaked for 10 min in a 10% ethanol/water solution, washed with sterilized deionized water, surface-sterilized for 20 min using a 20% bleach/water solution, and then washed several times with sterilized deionized water. Surface-sterilized seeds were germinated upon 2.4 g of sterilized filter paper moistened with 8 mL

* To whom correspondence should be addressed. Telephone: 785-532-6124. Fax: 785-532-7278. E-mail: ldavis@ksu.edu.

† Current address: Department of Chemistry, University of Texas at El Paso, 500 W. University, El Paso, TX, 79968.

10.1021/jf072052e CCC: $37.00 
Published on Web 11/30/2007

**Table 1.** Assignment of the Main IR Bands in IR Spectra of Sunflower and Maize Secondary Roots

| band | assignment | frequency range ($cm^{-1}$) | comments |
|---|---|---|---|
| A[a] | asymmetric $CH_3$stretch | 2940−2960 | lipids; exact frequency varies on attached groups |
| B[a] | asymmetric $CH_2$ stretch | 2910−2930 | lipids; exact frequency varies on attached groups |
| C[a] | symmetric $CH_3$ stretch | 2860−2885 | lipids; exact frequency varies on attached groups |
| D[a] | symmetric $CH_2$ stretch | 2840−2860 | lipids; exact frequency varies on attached groups |
| E[a,b] | C═O stretching of carboxyl ester (alkyl) | ≈1740 | lipids; exact frequency varies on attached groups, esterified pectins |
| F[b] | C═O stretching of phenolic ester | ≈1720 | phenolics; because of lipids or uronic acids |
| G[c] | amide I: C═O stretch plus C−N stretch | ≈1650 | protein; exact frequency based on secondary structure |
| H[b] | aromatic C═C stretch | ≈1635 | hydrocinnamic acid in lignin |
| I[b,d] | $COO^-$ asymmetric stretch | ≈1600 | acidic groups of pectic polysaccharides |
| J[c] | amide II: N−H deformation plus C−N stretch | ≈1550 | protein; exact frequency based on secondary structure |
| K[b,d] | C═C phenolic stretch | ≈1515 | guaiacyl ring of lignin |
| L[e] | C−H bend of $OCH_3$ | 1445−1460 | cellulose and/or pectin |
| M[b] | C−H bends from asymmetric $CH_3$ | 1410−1420 | lipids, polysaccharides, and cellulose |
| N[b] | C−H bends from symmetric $CH_3$ | 1395−1364 | lipids, polysaccharides, and cellulose |
| O[b] | C−O−H deformation asymmetric C−C−O stretch of ester | 1240−1250 | diagnostic peak for hemicellulose or cellulose |
| P[d] | | 1200−900 | carbohydrate fingerprint region; very complex and depends upon contributions from polysaccharides, cellulose, hemicellulose, and pectins |
| Q[f] | aromatic C−H wag of the para-substituted benzene ring | ≈845 | aromatic ring associated with lignin or lignin monomers |

[a] From ref *15*. [b] From ref *20*. [c] From ref *24*. [d] From ref *25*. [e] From ref *27*. [f] From ref *26*.

of sterilized tap water inside sterilized Petri dishes. Five seeds were placed in each Petri dish, and each dish was sealed with parafilm. The placement of the seeds into Petri dishes was conducted on a sterilized benchtop in a small room adjacent to the laboratory that had no air circulation and no prior history of fungal growth. The germination time for both procedures was 5−7 days. After the germination period, only the healthy seedlings were transferred to amber stock jars containing 1X Hoagland's hydroponic nutrient solution prepared as previously described by Castro et al. (*22*). Amber stock jars were used to deter algal growth. The seedlings were suspended in the amber stock jars using polyurethane foam plugs; therefore, only the roots were in contact with the hydroponic growth solution. The seedlings were then placed under 40 W cool white fluorescent tubes (about 1 tube/$ft^2$) with continuous lighting for 2 weeks (14 days). During this period, the solution level was maintained nearly constant by adding fresh 1X Hoagland's solution every day. After the 2 week growth period, the roots were rinsed with deionized (DI) water to remove any residual hydroponic solution. The roots were then cryosectioned in preparation for analysis by SR−IMS.

**Methods.** *Cryosectioning of Plant Roots for SR−IMS.* Cryosectioning of the root tissue was conducted on an IEC minotome with cryostat (Triangle Biomedical Sciences, Durham, NC) at the Diagnostic Laboratory at the College of Veterinary Medicine located on the campus of Kansas State University. The representative roots from each treatment were pooled (∼5 roots/treatment), and samples were dissected in 1 cm sections from the tip. The root tissues were frozen onto specimen blocks surrounded by Tissue Tek (Sakura Finetek USA, Inc., Torrance, CA) at −40 °C, in preparation for sectioning at −20 °C. The 4 $\mu$m thick frozen sections were thaw-mounted onto infrared-reflecting "E" glass microscope slides (Smiths Detection, Danbury, CT). The slides were then stored at room temperature until analysis.

*SR−IMS.* SR−IMS was conducted at the National Synchrotron Light Source (NSLS) at Brookhaven National Laboratory (BNL) in Upton, NY, using a Nicolet NicPlan infrared (IR) microscope and Thermo-Nicolet Magna 860 spectrometer equipped with a KBr beamsplitter on beamline U2B. The narrow-range, internal mercury cadmium telluride (MCT/A) detector was used, covering a range of 4000–650 $cm^{-1}$. Collimated synchrotron light with a beam energy of 800 MeV is passed through an external beam pipe into the IR microspectrometer to perform reflection spectroscopy. The IR spectra were collected in absorption mode at a resolution of 4 $cm^{-1}$ with 64 scans co-added to increase the signal-to-noise ratio. Each spectrum is ratioed to a reference, taken at an empty part of the low "E" slide, which was recorded with the same parameters and conditions (128 scans used for reference). A 30 $\mu$m square aperture was used for scouting potential specimens for mapping and taking individual spectra. A 12 × 12 $\mu$m square aperture with 10 $\mu$m steps was used for generating an IR map of root sections using the Atl$\mu$s, a component of the Omnic 6.0 software package (Thermo-Electron, Madison, WI) used to control the microscope stage. The optics were purged using dry $N_2$ to minimize absorption of $CO_2$ and water vapor in the ambient air. SR−IMS spectra were expressed as $\log(1/R)$ (equal to absorbance), and a baseline correction was used to generate the final spectra.

Specific regions of root tissue were selected for line and area mapping using Atl$\mu$s. The motorized computer-controlled microscope stage traced the designated tissue area for sampling into a *xy* grid for the synchrotron beam to follow. IR spectra were taken by a point-by-point sequence across the designated area to form a *xy* surface that corresponded to the morphology of the sample and a *z* direction containing the spectral information. The resulting data can be displayed as a series of spectroscopic images collected at individual wavelengths or as a series of IR spectra obtained at each pixel position of the image mapped. The spectra from the dataset were area-normalized to compensate for changes in thickness across the section. Functional group images were produced by plotting the intensity of the IR spectral bands as a function of the *xy* position. False color intensity maps were derived from the area under particular spectral features. An intensity ruler, which depicts the absorption intensity of a particular functional group, is shown directly under each area and line map. The red color represents high intensity, and the blue color stands for little or no intensity. The blue lines or rectangles on the visible image of each root section represent the area studied. The number of samples and areas examined varied because of the limited synchrotron beam time as well as the status of the synchrotron beam.

*PCA.* PCA of the FTIR spectra was performed using the WINDAS software package (*23*). In brief, a construct matrix that consists of the raw preprocessed spectra obtained from the maize and sunflowers samples was used to construct and test the model. Two-thirds of the spectra was used as the training set to develop the model, and one-third of the spectra was used to test the model. The fingerprint region from 1800 to 700 $cm^{-1}$ was used for the PCA of all of the samples. A single point baseline correction was performed at 1800 $cm^{-1}$, followed by area normalization of the region of 1800–700 $cm^{-1}$. The groups defined for the training sets were established on the basis of the region of root tissue (epidermis, cortex, or vascular region). The spectra for the respective groups are selected and placed into a data matrix. The data matrix was compressed using the covariance matrix method, and the principal components (PC) were calculated from the eigenvalues of the covariance matrix. PC score plots were created to show the distribution of the samples. The training set was then used to develop the model using linear discriminant analysis (LDA) and the squared Mahalanobis distance metric (*23*). The group center was calculated for each dataset, and the distance of each sample from its group center was determined. The result became the model. The spectra or samples

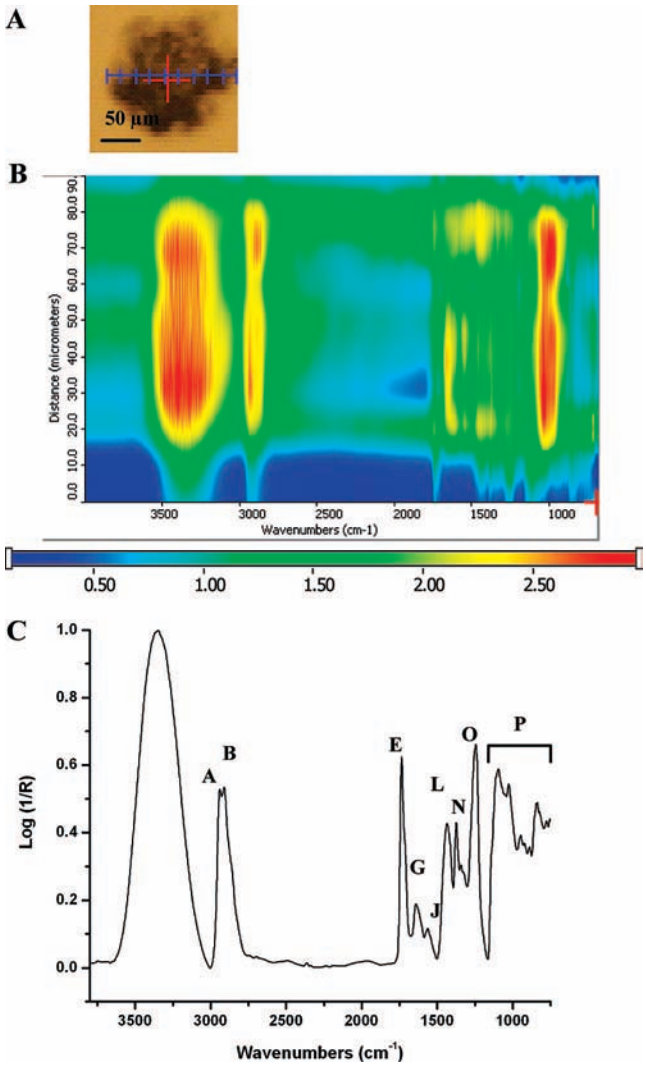


**Figure 1.** Line map and typical IR spectrum of the sunflower root cap approximately 100 $\mu$m from the root tip. (**A**) Visible image of the root cap. (**B**) False color intensity line map of the root cap. Line length = 120 $\mu$m. The blue line indicates the line mapped starting from the right and ending on the left. (**C**) Typical spectrum of the sunflower root cap tissue. The spectrum is an average of 10 root cap spectra. The spectra were normalized to the carbohydrate region between 1150 and 1000 cm$^{-1}$. Refer to **Table 1** for a description of band assignments.

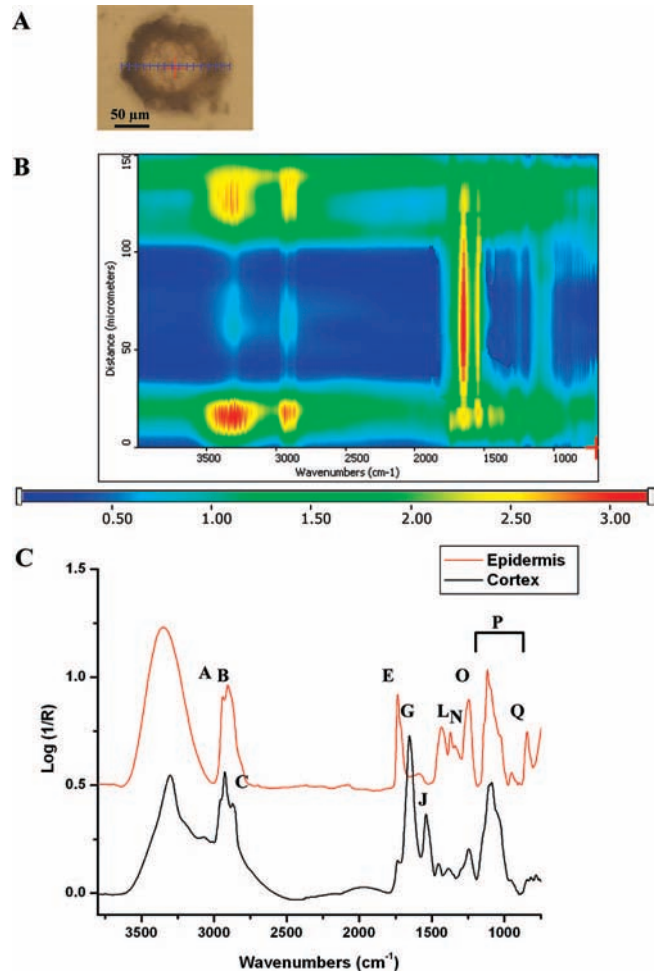


**Figure 2.** Line map and typical IR spectrum of the sunflower root approximately 250 $\mu$m from the root tip. (**A**) Visible image of the root section. (**B**) False color intensity line map of the root section. Line length = 150 $\mu$m. The blue line indicates the line mapped starting from the right and ending on the left. (**C**) Typical spectrum of the sunflower root cortex (black) and epidermis (red) tissue (listed from the bottom to the top). Each spectrum is an average of 10 spectra. The epidermis spectra were normalized to the OH peak at 3350 cm$^{-1}$, and the cortex spectra were normalized to the amide II band at 1650 cm$^{-1}$. Refer to **Table 1** for a description of band assignments. Spectra are arbitrarily offset for ease of presentation.

designated for the test set were then used to test the robustness of the model. Each sample was assigned to a group based on its proximity to a particular group center. Those samples that fall outside of the 95% tolerance region were considered unassigned. The robustness of the model was determined by the successful assignment of the samples from the test set to their proper group.

## RESULTS AND DISCUSSION

**Assignment of IR Bands in Maize and Sunflower Root Tissue.** The assignment of the main IR bands found in sunflower and maize secondary roots grown hydroponically in Hoagland's solution are displayed in **Table 1**. IR bands mainly associated with lipids are located between 3000 and 2800 cm$^{-1}$ (bands A−D) and correspond to asymmetric and symmetric stretches of $CH_3$ and $CH_2$ (*15*). Carbonyl stretches of carboxyl and phenolic esters at 1740 cm$^{-1}$ (band E) and 1720 cm$^{-1}$ (band F), respectively, also signify the presence of lipids and lignin (*7, 15, 20*). Proteins are represented by IR bands near 1650 cm$^{-1}$ (amide I, band G) and 1550 cm$^{-1}$ (amide II, band J) because of the amide linkage (*24*). The aromatic rings of lignin give rise to IR bands from C=C stretching at 1635 cm$^{-1}$ (band H) (*20*) and 1515 cm$^{-1}$ (band K) (*20, 25*) and a sharp band at 845 cm$^{-1}$ (band Q) (*26*). IR bands from polysaccharides, cellulose, and carbohydrates overlap in the carbohydrate fingerprint region of 1200–900 cm$^{-1}$ (band P) (*25*). Kacurakova et al. (*27*) have studied purified cell-wall polysaccharides and have determined some major peaks, which can aid in identifying some key polysaccharides in root tissue. There are also some regions of overlap with components of polysaccharides, cellulose, and lipids in the region of 1447–1459 cm$^{-1}$ (band M) and 1395–1364 cm$^{-1}$ (band N) representing C−H bends of symmetric and asymmetric $CH_3$ (*20, 27*). However, there are several diagnostic peaks for cellulose, which are located at 1240 cm$^{-1}$ (band O) (*4, 20, 27*) and 1420 cm$^{-1}$ (band L) (*4, 28*) and correspond to C−O−C vibrations and C−C ring stretching, respectively. The presence of many types of polysaccharides in plants makes it difficult to make an exact qualitative assessment of which polysaccharides are present in the root tissue.

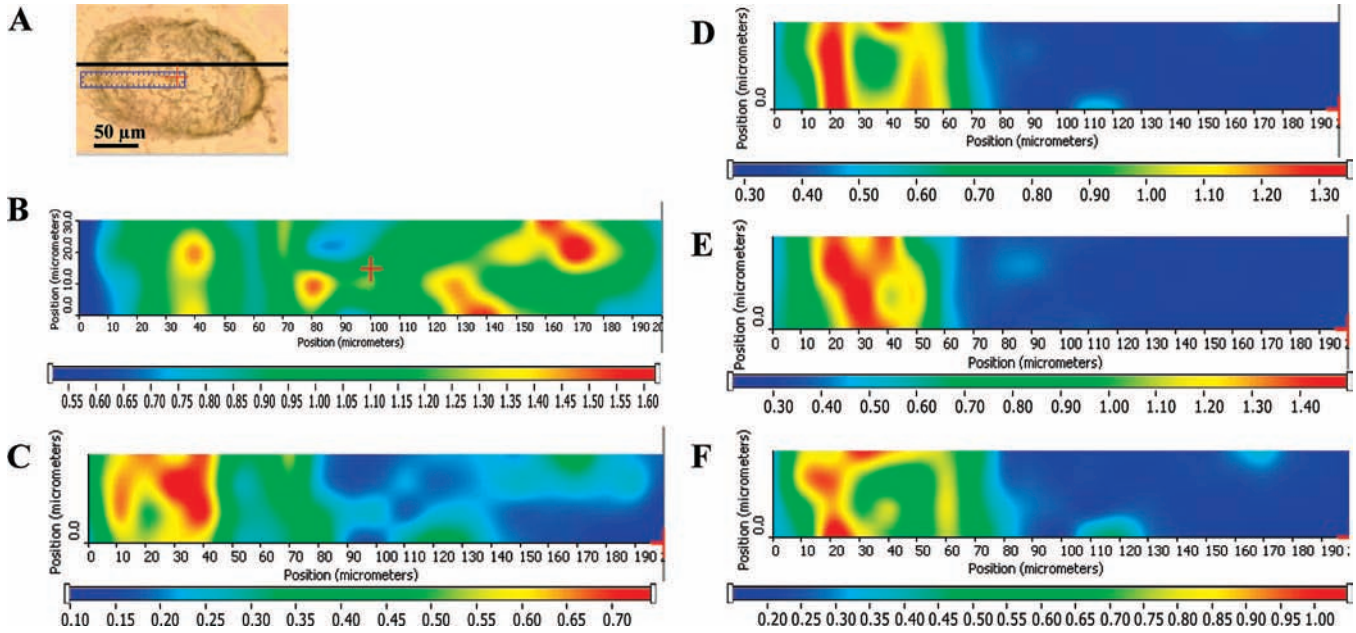


**Figure 3.** Functional group area maps of the sunflower root tissue approximately 500 $\mu$m from the root tip. Dimensions of the area studied = 200 × 30 $\mu$m. Functional group images were produced by plotting the area under the IR spectral band as a function of the *xy* position. The intensity ruler is displayed under each functional group map. (**A**) Visible image of the root section. The blue rectangle denotes the area studied. (**B**) Area under the peak centered at 1650 cm$^{-1}$, representing the protein concentration and distribution. (**C**) Area under the peak at 1735 cm$^{-1}$ (C═O esters), showing the concentration and distribution of lipids. (**D**) Area under peaks at 1240 cm$^{-1}$, indicating the concentration and distribution of cellulosic material. (**E**) Area under peaks between 1200 and 1000 cm$^{-1}$, indicating the concentration and distribution of carbohydrates. (**F**) Area under the peak at 845 cm$^{-1}$, signifying the distribution and concentration of lignin.

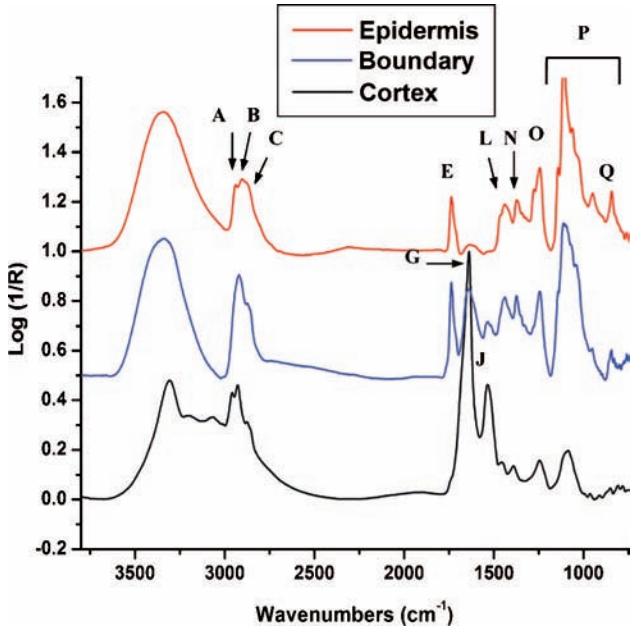


**Figure 4.** Typical spectrum of the sunflower root cortex (black), boundary between the epidermis and cortex (blue), and epidermis (red) tissue approximately 500 $\mu$m from the tip (listed from the bottom to the top). Each spectrum is an average of 10 spectra. The epidermis and boundary tissue spectra were normalized to the OH peak at 3350 cm$^{-1}$, and the cortex spectra were normalized to the amide II band at 1650 cm$^{-1}$. Refer to **Table 1** for a description of band assignments. Spectra are arbitrarily offset for ease of presentation.

**Infrared Dissection of Sunflower Root Tissue. Figures 1−8** depict spectra and line or area maps of functional groups of sunflower secondary root tissue at different distances from the root cap. They show the distribution and relative concentration of specific biopolymers associated with particular root structural components. Representative spectra shown in **Figures 1−8** display the different spectral characteristics associated with a particular structural component of secondary root tissue.

**Figure 1** shows a line map of the sunflower root cap approximately 100 $\mu$m from the root tip. The intensities of the peaks under each spectrum are constant throughout the line studied, meaning that the root cap is fairly homogeneous in structure. A representative spectrum of root cap tissue (**Figure 1C**) shows that the root cap is dominated by the carbohydrate fingerprint region (band P). This is to be expected because root caps of dicots excrete pectic polysaccharides and arabinogalactan proteins (AGPs) (*29*) and often contain starch grains. Because there are many overlaps in the carbohydrate fingerprint region, some peaks represent more than one type of polysaccharide. The strong peak at 1080 cm$^{-1}$ is commonly found in spectra of arabinogalactan (*28*) and in pectins. Further confirmation of pectin or pectic polysaccharides is denoted by peaks at 1418 (band L), 953, 890, and 833 cm$^{-1}$. The strong peak at 1025 cm$^{-1}$ is indicative of starch (*28*), and peaks at 1240 and 1373 cm$^{-1}$ (bands O and N) are diagnostic for cellulose. Bands G (amide I) and J (amide II) reflect the obvious presence of protein, while the presence of lipids is represented by bands A, B, and E.

**Figure 2** presents the line map of the root cap approximately 250 $\mu$m from the root tip, near the apical meristem. Two distinct regions representing the epidermis and cortex can be observed. The cortex is more proteinaceous (bands G and J) and, overall, contains less lipid than the epidermis. The spectrum of the epidermis (**Figure 2C**) has sharp peaks at 1740 cm$^{-1}$ (band E, C═O ester) and 845 cm$^{-1}$ (band Q), a peak diagnostic for some types of lignin (mainly ferulic acid). The epidermis also has a higher relative concentration of cellulose (bands L, N, and O) and pectin (band L). However, both still maintain pectic polysaccharide and starch components similar to those seen in the root cap because the root tissue at 250 $\mu$m is still

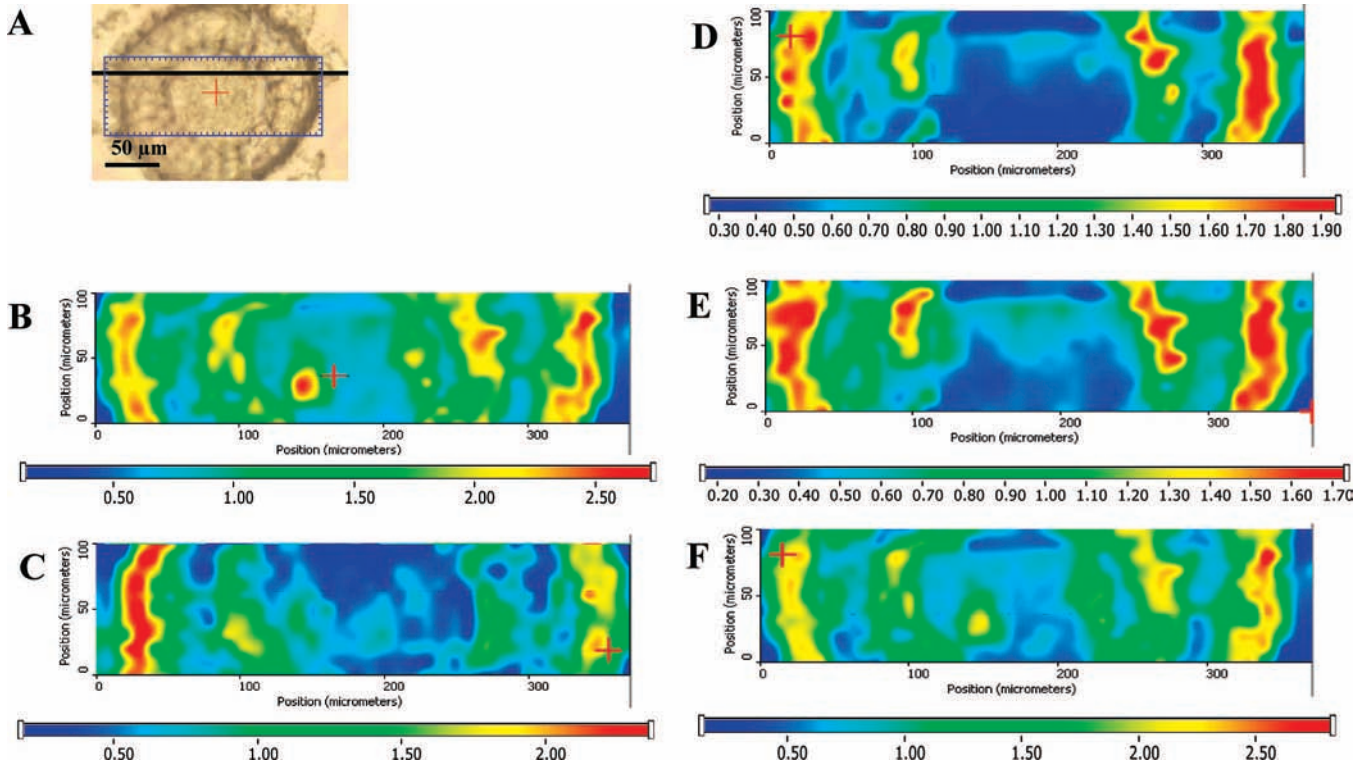


**Figure 5.** Functional group area maps of the sunflower root tissue approximately 1 mm from the root tip. Dimensions of the area studied = 350 × 100 $\mu$m. Functional group images were produced by plotting the area under the IR spectral band as a function of the *xy* position. The intensity ruler is displayed under each functional group map. (**A**) Visible image of the root section. The blue rectangle denotes the area studied. (**B**) Area under the peak centered at 1650 cm$^{-1}$, representing the protein concentration and distribution. (**C**) Area under the peak at 1735 cm$^{-1}$ (C═O esters), showing the concentration and distribution of lipids. (**D**) Area under peaks at 1240 cm$^{-1}$, indicating the concentration and distribution of cellulosic material. (**E**) Area under peaks between 1200 and 1000 cm$^{-1}$, indicating the concentration and distribution of carbohydrates. (**F**) Area under the peak at 845 cm$^{-1}$, signifying the distribution and concentration of lignin.

predominantly made of root cap tissue, with cells beginning to differentiate into vascular tissue.

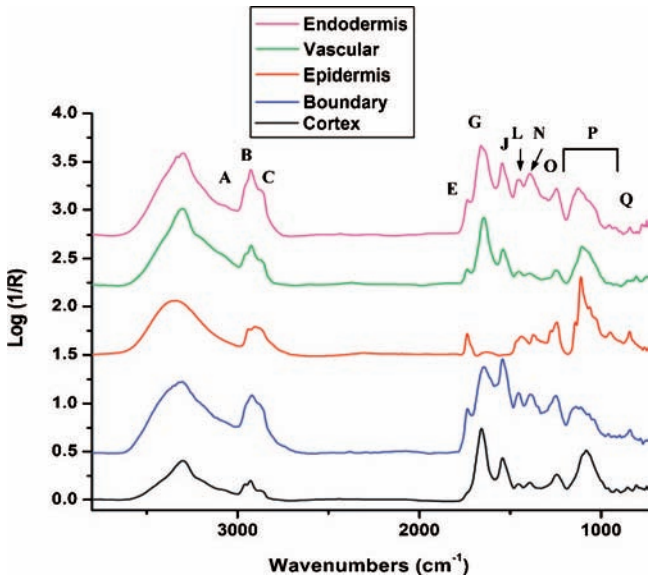


**Figure 6.** Typical spectrum of the sunflower root cortex (black), boundary tissue between the epidermis and cortex (blue), epidermis (red), vascular tissue (green), and endodermis (purple) approximately 1 mm from the root tip (listed from the bottom to the top). Each spectrum is an average of 10 spectra. The epidermis, endodermis, boundary, and vascular tissue spectra were normalized to the OH peak at 3350 cm$^{-1}$, and the cortex spectra were normalized to the amide II band at 1650 cm$^{-1}$. Refer to **Table 1** for a description of band assignments. Spectra are arbitrarily offset for ease of presentation.

**Figure 3** shows the functional group area maps of sunflower root tissue about 500 $\mu$m from the root tip. The spatial protein distribution and concentration is depicted in the functional group map of the area under peaks centered at 1650 cm$^{-1}$ (**Figure 3B**). The protein is mostly concentrated in the center of the cortex region, where it appears that the organization of the vascular tissue is beginning to take place. The spatial distribution of lipids is concentrated in the epidermis as seen in the functional group map of the area under the peak centered at 1740 cm$^{-1}$ (C═O ester) in **Figure 3C**. A similar pattern of distribution can also be seen for cellulose (**Figure 3D**), carbohydrates (**Figure 3E**), and lignin (**Figure 3F**). These observations can be confirmed by examining the spectra of cortex, epidermis, and boundary tissue between the cortex and epidermis in **Figure 4**. The spectrum of boundary tissue resembles a mixture of cortex and epidermis, containing protein, lipid, and lignin functionalities. Both epidermis and boundary tissues possess arabinogalactan-type polysaccharides (band P) and starch. The carbohydrate fingerprint region (band P) of the cortex spectrum resembles a similar pattern to xyloglucan (*28*), a noncellulosic polysaccharide found in most angiosperms that is a major component in cell walls of suspension cultured dicots (*30*).

**Figure 5** presents the functional group area maps of sunflower root tissue about 1 mm from the root tip. At this distance, the endodermis has begun to form. A similar distribution of proteins (**Figure 5B**), lipids (**Figure 5C**), cellulose (**Figure 5D**), carbohydrates (**Figure 5E**), and lignin (**Figure 5F**) is concentrated in the boundary tissue and endodermis. There is a circular area of protein concentrated in the vascular tissue (inside the endodermis) that overlaps with the lignin distribution, which

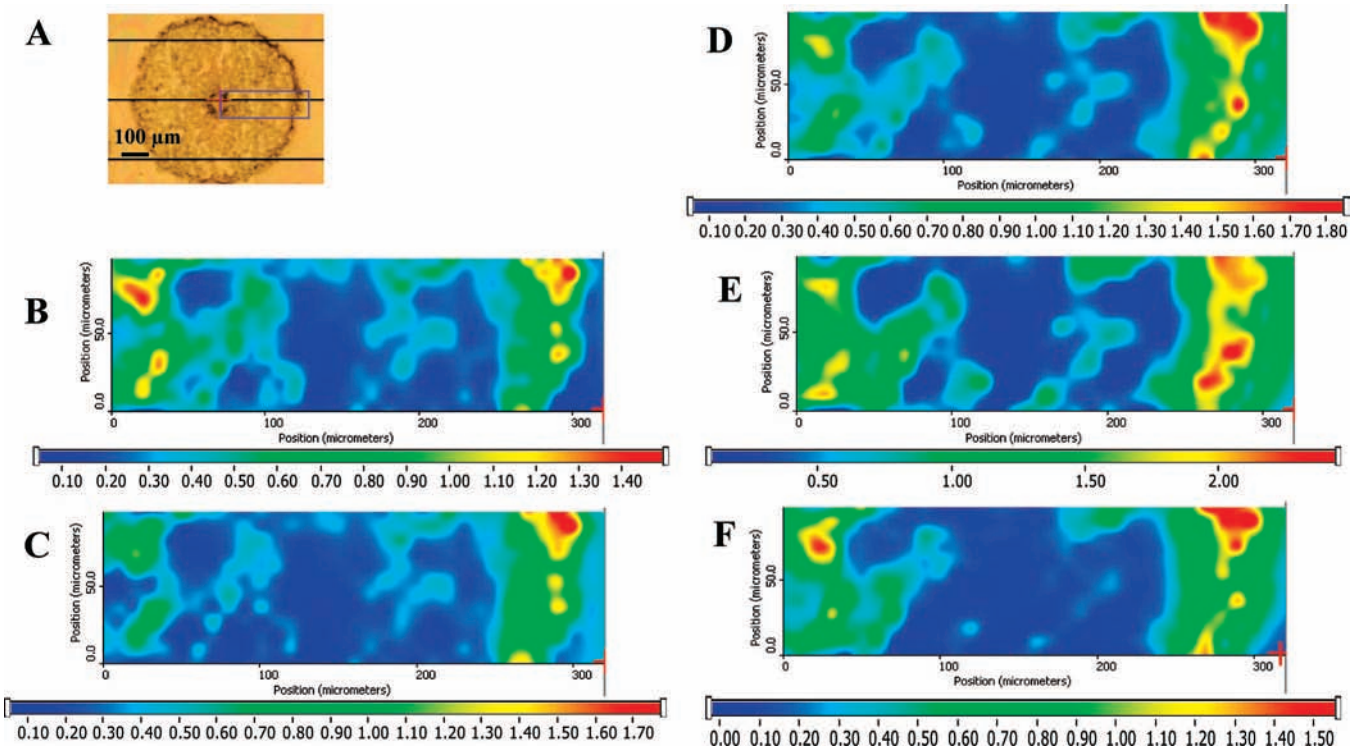


**Figure 7.** Functional group area maps of the sunflower root tissue approximately 1 cm from the root tip. Dimensions of the area studied = 320 × 90 $\mu$m. Functional group images were produced by plotting the area under the IR spectral band as a function of the *xy* position. The intensity ruler is displayed under each functional group map. (**A**) Visible image of the root section. The blue rectangle denotes the area studied. (**B**) Area under the peak centered at 1650 cm$^{-1}$, representing the protein concentration and distribution. (**C**) Area under the peak at 1735 cm$^{-1}$ (C═O esters), showing the concentration and distribution of lipids. (**D**) Area under peaks at 1240 cm$^{-1}$, indicating the concentration and distribution of cellulosic material. (**E**) Area under peaks between 1200 and 1000 cm$^{-1}$, indicating the concentration and distribution of carbohydrates. (**F**) Area under the peak at 845 cm$^{-1}$, signifying the distribution and concentration of lignin.

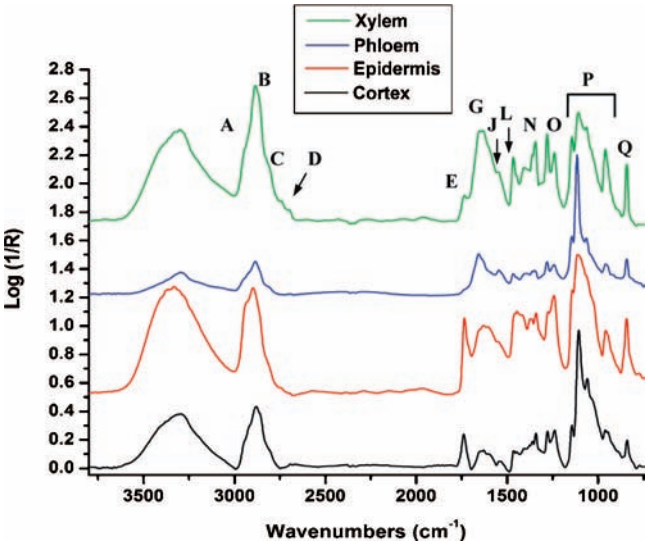


**Figure 8.** Typical spectrum of the sunflower root cortex (black), epidermis (red), and phloem (blue), and xylem (green) tissue approximately 1 cm from the tip (listed from the bottom to the top). Each spectrum is an average of 10 spectra. All spectra were normalized to the carbohydrate region between 1150 and 1000 cm$^{-1}$. Refer to **Table 1** for a description of band assignments. Spectra are arbitrarily offset for ease of presentation.

may signify the development of a xylem vessel. The spectra of the different structural components in the root at 1 mm are displayed in **Figure 6**. The spectrum of vascular tissue is similar to the cortex but has a relative higher concentration of lipids because of the higher intensities of bands A, B, C, E, and N. Also, the lignin peak at 845 cm$^{-1}$ (band Q) is twice as intense in the spectrum of vascular tissue when compared to the spectrum of the cortex. The endodermis has features similar to the boundary tissue but is more proteinaceous. The epidermis and cortex are relatively unchanged when compared to the root at about 500 $\mu$m.

**Figure 7** shows the functional group area maps of sunflower root tissue about 1 cm from the root tip where the vascular region has fully developed xylem and phloem. The spatial distribution of lipids (**Figure 7C**), cellulose (**Figure 7D**), carbohydrates (**Figure 7E**), and lignin (**Figure 7F**) are most concentrated in the xylem, followed by the epidermis, and, to a lesser degree, in the phloem. This is expected because the xylem is very thick and highly lignified, thus providing structure for the root and the passage for water and minerals to the aerial parts of the plants. There is also a high concentration of protein (**Figure 7B**) in the xylem coinciding with lignin (**Figure 7F**) deposition. This same overlapping pattern of protein and lignin was also observed at 1 mm. **Figure 8** shows the spectra of the different structural components observed at 1 cm. Because of the lignification of the xylem, there is an intense peak representing phenolic or aromatic compounds at 845 cm$^{-1}$ (band Q). Also, the xylem IR spectrum has peaks for lipids (bands A, B, C, D, E, M, and N) and cellulose (bands L, M, N, and O). The peaks in the carbohydrate fingerprint region (band P) are similar to those indicative of arabinogalactan and pectic polysaccharides. Intense peaks at 1282 and 953 cm$^{-1}$ are related to pectic- and xyloglucan-type polysaccharides, respectively (*28*). The IR spectrum of the phloem contains the same IR bands observed in the xylem but with less intensity. However, the phloem IR spectrum has a different band pattern in the carbohydrate

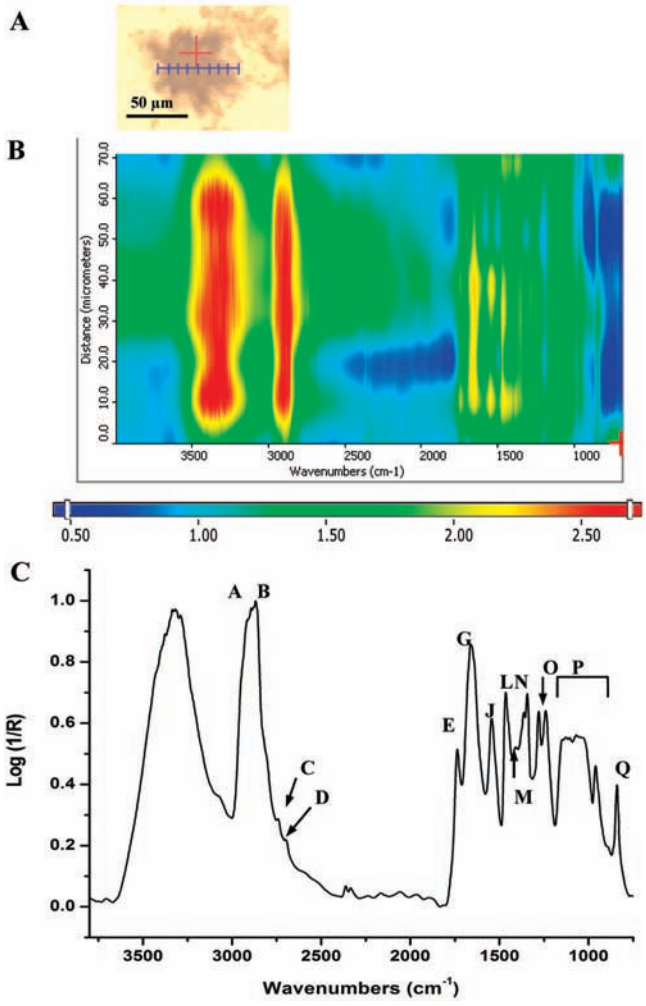


**Figure 9.** Line map and typical IR spectrum of maize root cap approximately 150 $\mu$m from the root tip. (**A**) Visible image of the root cap. (**B**) False color intensity line map of the root cap. Line length = 70 $\mu$m. The blue line indicates the line mapped starting from the right and ending on the left. (**C**) Typical spectrum of maize root cap tissue. The spectrum is an average of 10 root cap spectra. The spectra were normalized to the OH peak at 3350 cm$^{-1}$. Refer to **Table 1** for a description of band assignments.

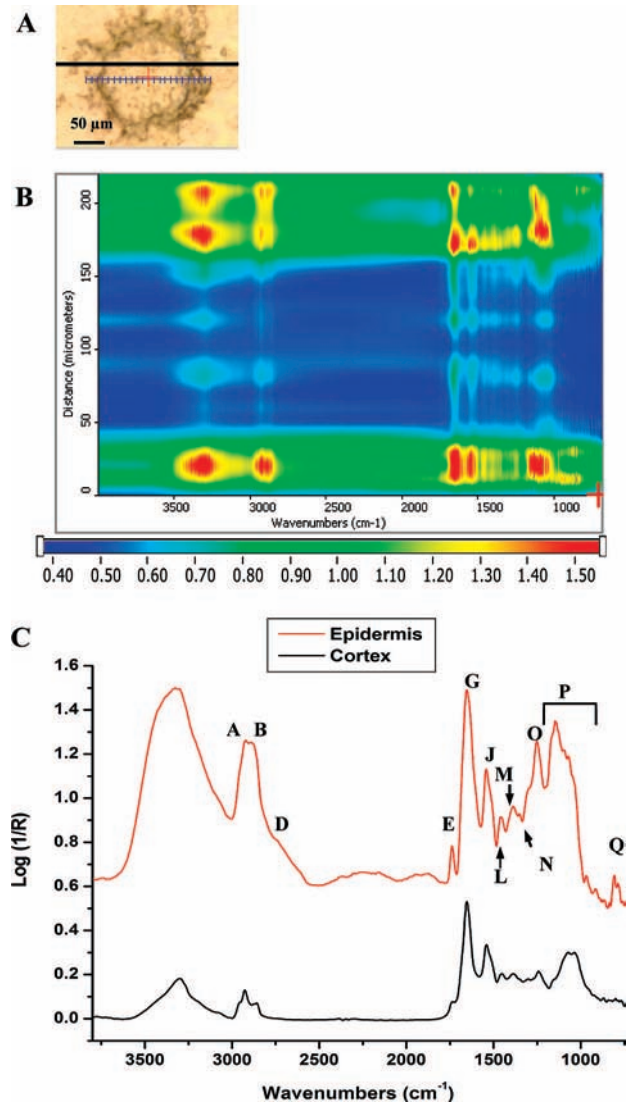


**Figure 10.** Line map and typical IR spectrum of the maize root approximately 400 $\mu$m from the root tip. (**A**) Visible image of the root section. (**B**) False color intensity line map of the root section. Line length = 220 $\mu$m. The blue line indicates the line mapped starting from the right and ending on the left. (**C**) Typical spectrum of the maize root cortex (black) and epidermis (red) tissue (listed from the bottom to the top). Each spectrum is an average of 10 spectra. The epidermis spectra were normalized to the OH peak at 3350 cm$^{-1}$, and the cortex spectra were normalized to the amide II band at 1650 cm$^{-1}$. Refer to **Table 1** for a description of band assignments. Spectra are arbitrarily offset for ease of presentation.

fingerprint region (band P), suggesting the presence of different polysaccharides. The epidermis spectrum also has the same IR peaks seen in the xylem and phloem. There is the appearance of protein bands not previously observed in the epidermis closer to the root tip. It is possible that the IR spectrum representing the epidermis may be a mixture of epidermis and exodermis (boundary tissue between the epidermis and cortex that contains proteins). The cortex spectrum contains lignin and lipid bands and lacks the intense amide I (band G) and amide II (band J) bands typically observed in the cortex closer to the tip. As it often occurs, older developed tissue may contain less protein and become more rigid and lignified.

**Infrared Dissection of Maize Root Tissue. Figures 9−14** depict spectra and line or area maps of functional groups of maize secondary root tissue at different distances from the root cap. The sampling of the maize tissue and generation of line and functional group area maps were conducted under the same conditions and parameters as previously discussed for sunflower secondary root tissue.

**Figure 9** represents a line map of the maize root cap approximately 150 $\mu$m from the root tip. As in the case of the sunflower root cap, the intensities of the peaks under each spectrum are fairly constant throughout the line studied, meaning that the root cap is fairly homogeneous in structure. A representative spectrum of root cap tissue (**Figure 9C**) shows that the root cap is dominated by lipid indicated by the presence of IR bands A, B, E, M, and N. IR bands L, M, N, and O denote the presence of cellulose. Maize root caps possess proteins signified by IR peaks at 1650 cm$^{-1}$ (band G) and 1550 cm$^{-1}$ (band J). A unique feature of maize plants is the presence of aromatic substances in nonlignified cell walls (*31*) indicated by the presence of a peak at 845 cm$^{-1}$ (band Q). These aromatic substances, such as ferulate and *p*-coumarate, are often found bound to lignin monomers and are cross-linked to pectic polysaccharides and heteroxylans (*32*). The pattern of IR bands in the carbohydrate fingerprint region (band P) is similar to that

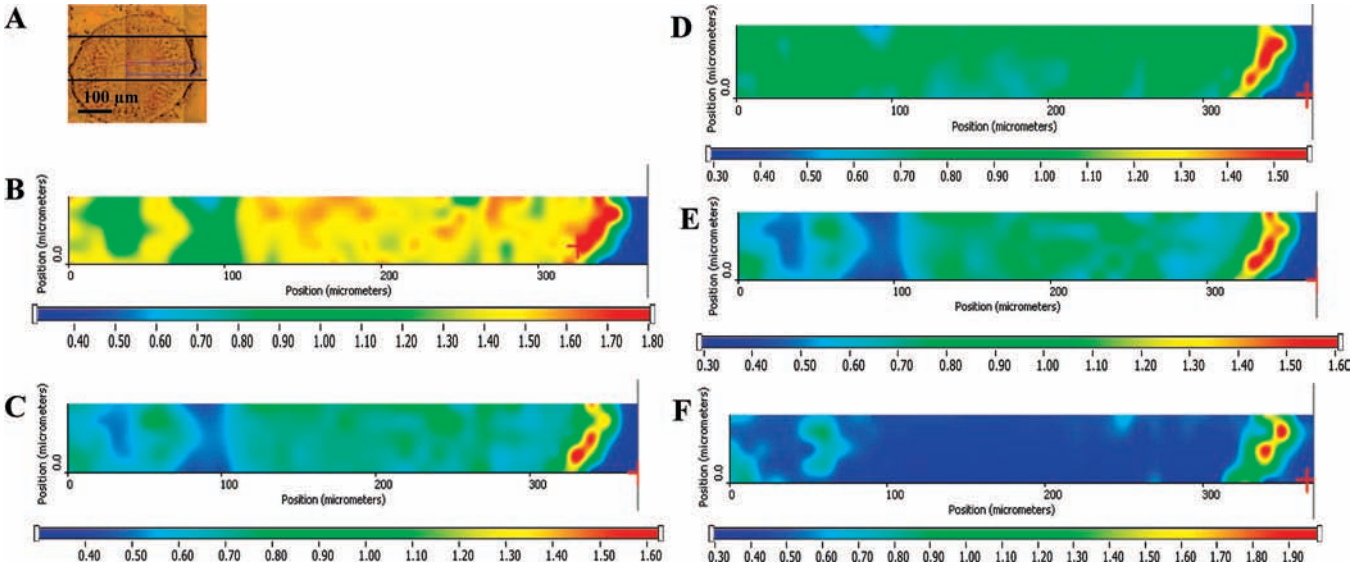


**Figure 11.** Functional group area maps of maize root tissue approximately 800 $\mu$m from the root tip. Dimensions of the area studied = 380 × 45 $\mu$m. Functional group images were produced by plotting the area under the IR spectral band as a function of the *xy* position. The intensity ruler is displayed under each functional group map. (**A**) Visible image of the root section. The blue rectangle denotes the area studied. (**B**) Area under the peak centered at 1650 cm$^{-1}$, representing the protein concentration and distribution. (**C**) Area under the peak at 1735 cm$^{-1}$ (C═O esters), showing the concentration and distribution of lipids. (**D**) Area under peaks at 1240 cm$^{-1}$, indicating the concentration and distribution of cellulosic material. (**E**) Area under peaks between 1200 and 1000 cm$^{-1}$, indicating the concentration and distribution of carbohydrates. (**F**) Area under the peak at 845 cm$^{-1}$, signifying the distribution and concentration of lignin.

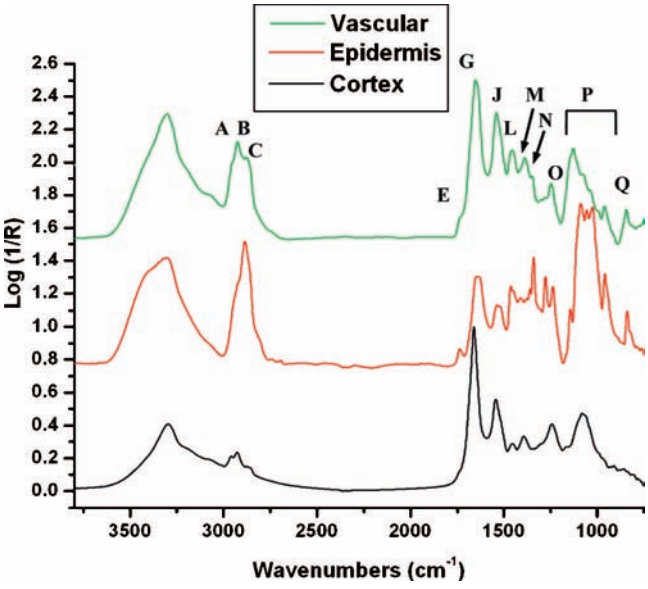


**Figure 12.** Typical spectrum of the maize root cortex (black), epidermis (red), and vascular tissue (green) approximately 800 $\mu$m from the root tip (listed from the bottom to the top). Each spectrum is an average of 10 spectra. The epidermis spectrum was normalized to the carbohydrate region between 1150 and 1000 cm$^{-1}$. The cortex and vascular tissue spectra were normalized to the amide II band at 1650 cm$^{-1}$. Refer to **Table 1** for a description of band assignments. Spectra are arbitrarily offset for ease of presentation.

of rhamnogalacturonan (*28*), a pectic polysaccharide found in cell walls of somatic cells in maize and rice (*31*). Also, intense peaks at 1282 and 953 cm$^{-1}$ indicate the presence of pectic- and xyloglucan-type polysaccharides, respectively. Xyloglucans are known to be present in cell walls in the root tips and meristematic cells of grasses (*31*).

**Figure 10** presents the line map of the maize root approximately 400 $\mu$m from the root tip. Two distinct regions in the line map can be observed, representing the epidermis and cortex. The most intense IR peaks can be found in the epidermis. There is a strong presence of protein, lipids, polysaccharides, cellulose, and aromatic compounds (because of lignin monomers cross-linked to pectic polysaccharides) in the epidermis (**Figure 10C**). IR bands associated with pectin and rhamnogalacturonan can be observed in the carbohydrate fingerprint region (band P). The cortex IR spectrum contains less intense peaks for lipids, proteins, and cellulose, and the lack of band Q (845 cm$^{-1}$) denotes the absence of lignin or lignin monomers. The IR bands in the carbohydrate fingerprint region, 1155, 1080, and 1040 cm$^{-1}$, are indicative of arabinogalactan and xyloglucan (*28*). Arabinogalactans are found in numerous cellular locations and are usually associated with plasma membrane and cell-wall compartments in grasses (*33*).

**Figure 11** shows the functional group area maps of maize root tissue about 800 $\mu$m from the root tip. The spatial distribution of protein (**Figure 11B**) shows that it is concentrated most heavily in the epidermis and slightly less throughout the cortex. There is a circular distribution of protein in the center of the root section, signifying the formation of xylem in the vascular tissue. The functional group maps for lipids (**Figure 11C**), cellulose (**Figure 11D**), carbohydrates (**Figure 11E**), and lignin (**Figure 11F**) show a concentrated distribution of these biopolymers in the epidermis. Cellulose is uniformly distributed throughout the cortex and vascular tissue. A circular distribution of lipids, carbohydrates, and lignin in the vascular tissue coincides with the distribution pattern of protein previously described. The spectra of the different structural components in the root at 800 $\mu$m are displayed in **Figure 12**. The representative spectrum of the cortex possesses the same IR peaks as the cortex spectrum at 400 $\mu$m. The carbohydrate fingerprint region dominates the epidermis IR spectrum, with peaks corresponding to pectin or pectic polysaccharides (1144, 1080, 1052, 1021, and 953 cm$^{-1}$), arabinogalactan (1144 and 1080 cm$^{-1}$), and xyloglucan (1282 cm$^{-1}$). The presence of pectin or pectic polysaccharides is also evidenced by band L (1458 cm$^{-1}$). The lipid peak in the region of 3000–2800 cm$^{-1}$

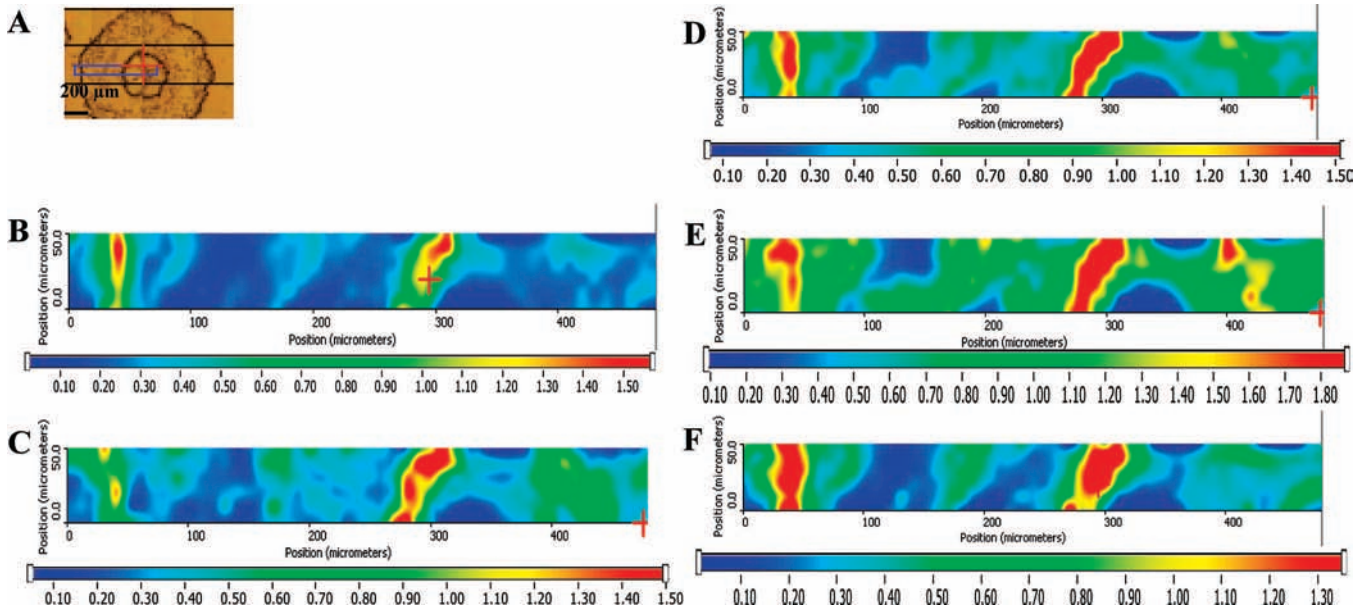


**Figure 13.** Functional group area maps of maize root tissue approximately 1 cm from the root tip. Dimensions of the area studied = 480 × 50 $\mu$m. Functional group images were produced by plotting the area under the IR spectral band as a function of the *xy* position. The intensity ruler is displayed under each functional group map. (**A**) Visible image of the root section. The blue rectangle denotes the area studied. (**B**) Area under the peak centered at 1650 cm$^{-1}$, representing the protein concentration and distribution. (**C**) Area under the peak at 1735 cm$^{-1}$ (C═O esters), showing the concentration and distribution of lipids. (**D**) Area under peaks at 1240 cm$^{-1}$, indicating the concentration and distribution of cellulosic material. (**E**) Area under peaks between 1200 and 1000 cm$^{-1}$, indicating the concentration and distribution of carbohydrates. (**F**) Area under the peak at 845 cm$^{-1}$, signifying the distribution and concentration of lignin.

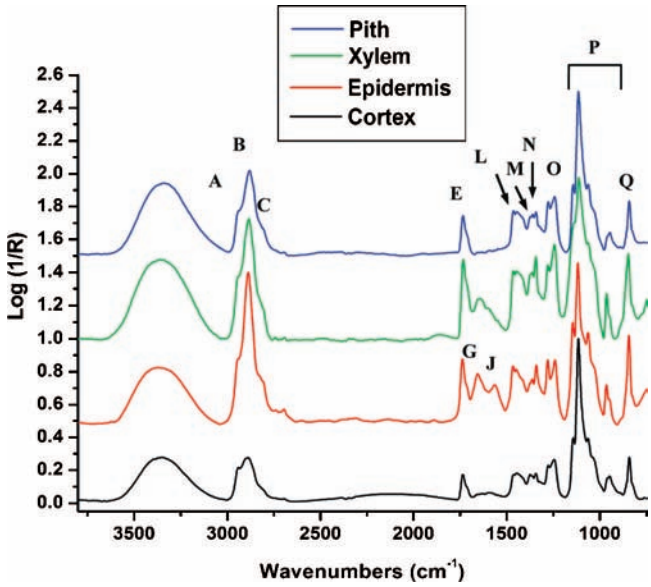


**Figure 14.** Typical spectrum of the maize root cortex (black), epidermis (red), xylem tissue (green), and pith (blue), approximately 1 cm from the root tip (listed from the bottom to the top). Each spectrum is an average of 10 spectra. All spectra were normalized to the carbohydrate region between 1150 and 1000 cm$^{-1}$. Refer to **Table 1** for a description of band assignments. Spectra are arbitrarily offset for ease of presentation.

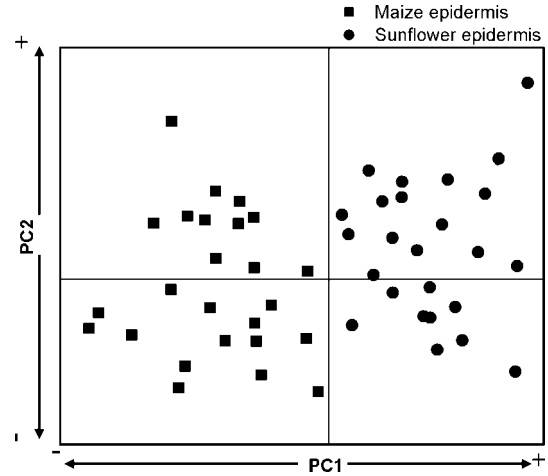


**Figure 15.** PCA score plot shows that maize and sunflower epidermis can be separated by the first 2 PCs.

is very intense particularly for band B (asymmetric $CH_3$ stretch). Lignification of the epidermis is marked by band Q.

**Figure 13** shows the functional group area maps of maize root tissue about 1 cm from the root tip where the vascular region has formed the typical xylem ring surrounding pith tissue. The spatial distribution of all of the biopolymers (parts **B**−**F** of **Figure 13**) is concentrated in the epidermis and xylem regions, with higher intensity in the xylem. The spectra of the different structural components in the root at 1 cm from the root tip are displayed in **Figure 14**. All of the structural components possess the same spectral features, with the exception of the IR bands attributed to protein. Only the spectra of epidermis and xylem contain bands G and J. The cortex has the least amount of overall intensity for all of the IR bands. The cortex at 1 cm contains little or no protein and contains IR bands not previously observed in the cortex at distances closer to the root tip. The degree of lignification has increased in all of the structural components, as shown by the sharp intense band at 845 cm$^{-1}$ (band Q). As the root develops, forming the xylem components, more and more lignin becomes deposited in the cell wall of tissues, especially in the xylem. The presence of band H in the xylem spectrum and higher peak intensity for band Q confirm that the xylem is more lignified than the other structural components. All of the structural components in the

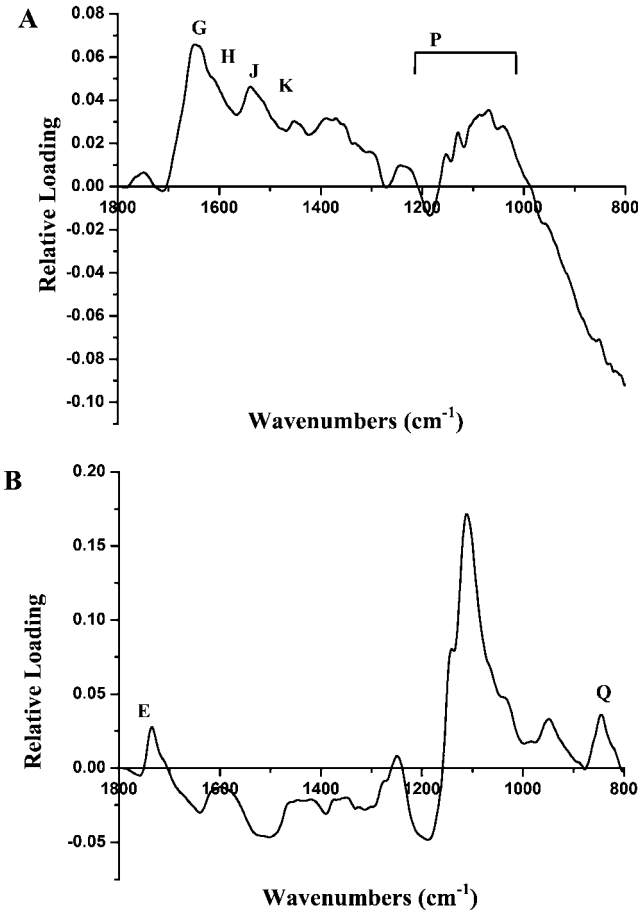


**Figure 16.** Loadings for the first (**A**) and second (**B**) PCs depicting the major variation between maize and sunflower epidermis spectra. The first PC loading contains IR bands from all of the biopolymers. The second PC loading mostly contains peaks from the carbohydrate fingerprint, 1200–900 $cm^{-1}$ (band P). Refer to **Table 1** for a description of band assignments.

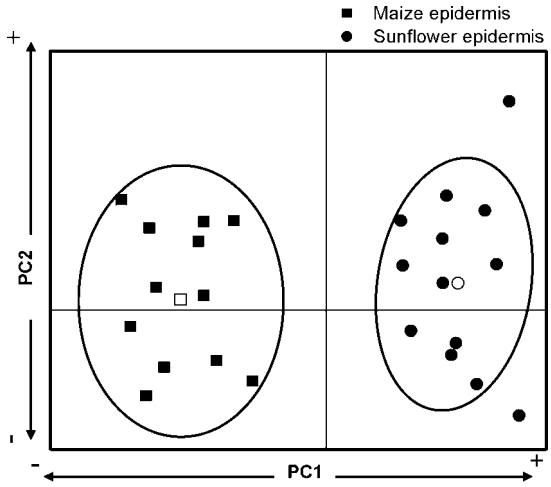


**Figure 17.** Validation plot used to test the robustness of the model set for maize and sunflower epidermis. The hollow symbols represent the (□) maize and (○) sunflower group centers. The ovals represent the 95% tolerance region. Two observations from the sunflower test set fell outside the 95% tolerance region and were not assigned to a group.

root at 1 cm also possess similar types of pectic polysaccharides, xyloglucan, and arabinogalactan, as corroborated by the IR peaks diagnostic for these biopolymers.

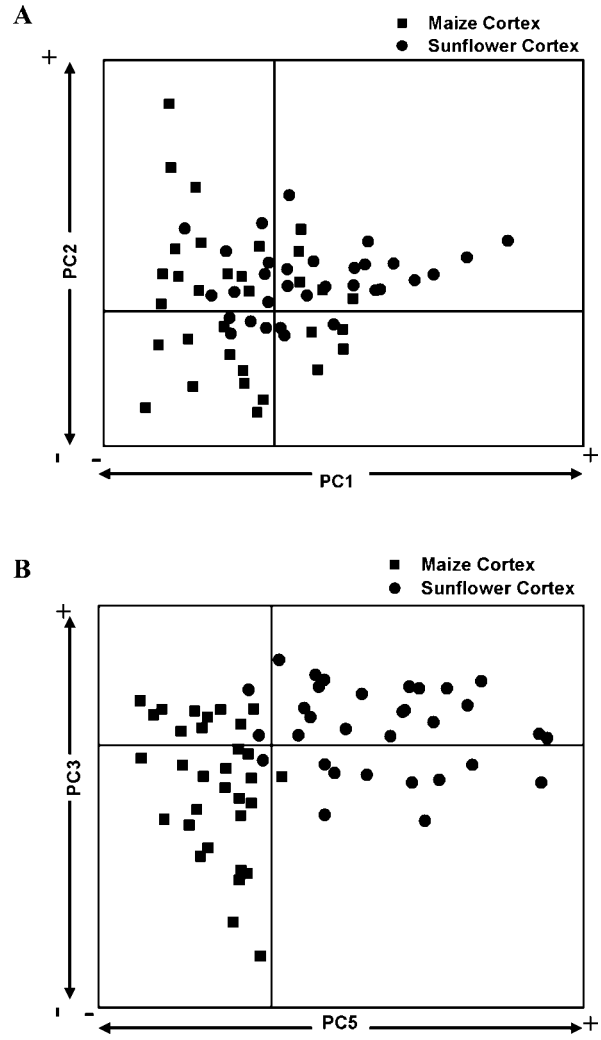


**Figure 18.** PCA score plots using the first and second PCs (**A**) and the third and fifth PCs (**B**). There no clear separation of the maize and sunflower cortex using PC1 and PC2. A good separation is achieved using the first and fifth PCs.

**Comparison of Maize and Sunflower Root Tissues.** Because all plant tissues are made of protein, cellulose, polysaccharides, lipids, and lignin and have similar IR spectral features, it can be difficult to visually distinguish between spectra of a particular structural component from two different plants. This issue may be resolved using PCA to uncover the most minor of differences between root tissues of hydroponically grown maize and sunflower plants. This section will discuss the ability of PCA to differentiate between the biopolymer makeup of the structural components of maize and sunflower root tissue using spectra from the epidermis, cortex, and xylem.

To compare the epidermis of the root tissue of maize and sunflower plants, spectra were randomly selected from spot, line, and area maps collected under the same experimental conditions. A total of 37 epidermal spectra were extracted from 12 different maize samples, and 38 epidermal spectra were obtained from 13 different sunflower samples that ranged in position from 400 $\mu$m to 1 mm from the root tip (this was the region with the most samples from both plants). Two-thirds of the spectra or observations was used for the training set, yielding 25 observations for each plant. A plot of the first two PCs (**Figure 15**) shows a distinct separation between maize and sunflower epidermal tissue by the first PC. The first two PC loadings seen in parts **A** and **B** of **Figure 16** account for 64 and 19% of the

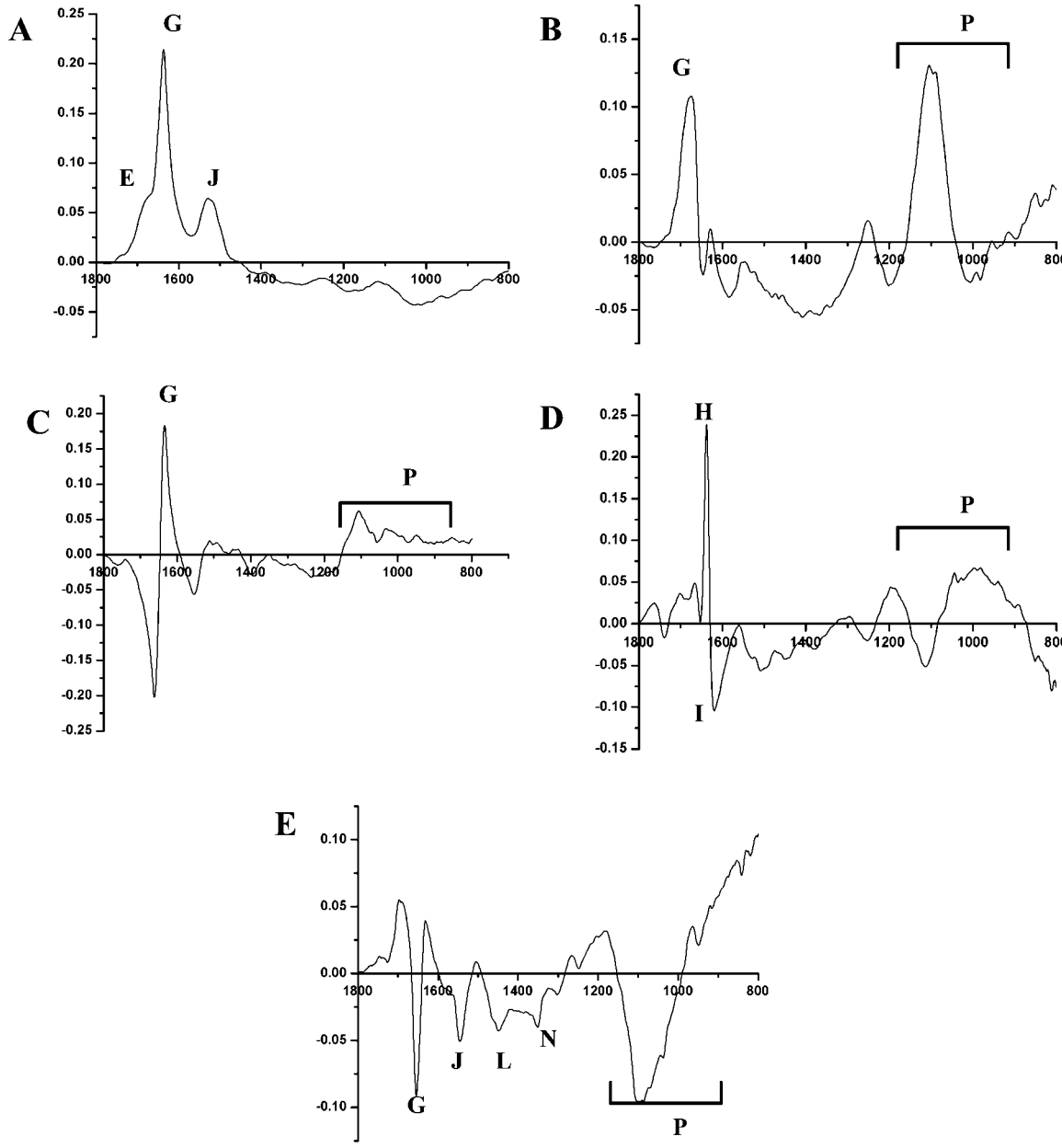


**Figure 19.** Loadings for the first (**A**), second (**B**), third (**C**), fourth (**D**), and fifth (**E**) PCs. The first and second PC loadings represent a combined 85% of the spectral variability. The third, fourth, and fifth PC loadings represent 2.88, 1.92, and 1.59% of the overall spectral variability. Refer to **Table 1** for a description of band assignments. The *x* axis represents frequency as wavenumbers ($cm^{-1}$), and the *y* axis represents relative loading.

variability between maize and sunflower epidermal spectra. Through inspection of the peaks present in PC1 (**Figure 16A**), maize appears to possess a higher concentration of proteins, lipids, lignin, and polysaccharides in its epidermis. Monocots, particularly grasses, contain more lignin than dicots, overall (*34*). It is also important to note that the lignin in dicots is typically composed of guaiacyl (G-type) and syringyl (S-type) rings, while the lignin in monocots, especially grasses, possesses G-, S-, and H- (hydrocinnamic acid) type rings (*35*). The positive presence of peaks because of the aromatic C═C stretch at 1635 $cm^{-1}$ (band H) and 1515 $cm^{-1}$ (band K), which appear as shoulders on the amide I and amide II peaks, and the positive peak at 845 $cm^{-1}$ (band Q) in the loading of PC2 (**Figure 16B**) provide evidence of this. The 1515 $cm^{-1}$ band corresponds to G- and S-type lignin, and the 1635 $cm^{-1}$ represents C═C stretching in the hydrocinnamic acid ring (*20*). The 1635 $cm^{-1}$ may be the most useful peak in distinguishing between maize and sunflower epidermis. The carbohydrate fingerprint region (band P) in the first PC loading does not represent one particular polysaccharide; however, it does signify that the maize root contains different types of polysaccharides than sunflower root tissue. This same region in the second PC loading has significantly positive peaks that correspond to arabinogalactans and possibly pectins. This is very plausible because the cell wall of maize seedlings are rich in arabinogalactans, some of which are in the form of AGPs (*31*). Using the first two PCs, linear discriminant analysis (LDA) resulted in a 100% correct assignment of the observations to their appropriate group. A total of 25 spectra (12 from maize root tissue and 13 from sunflower root tissue) from independent samples of maize and sunflower root tissue were used as the test set. On the basis of the Mahalanobis distance metric, the group centers were calculated from the training set. A validation plot was generated (**Figure 17**), displaying the distance of each sample from its particular group center forming the model. Two of the samples from the sunflower test set were considered unclassified because they lie outside the 95% tolerance region.

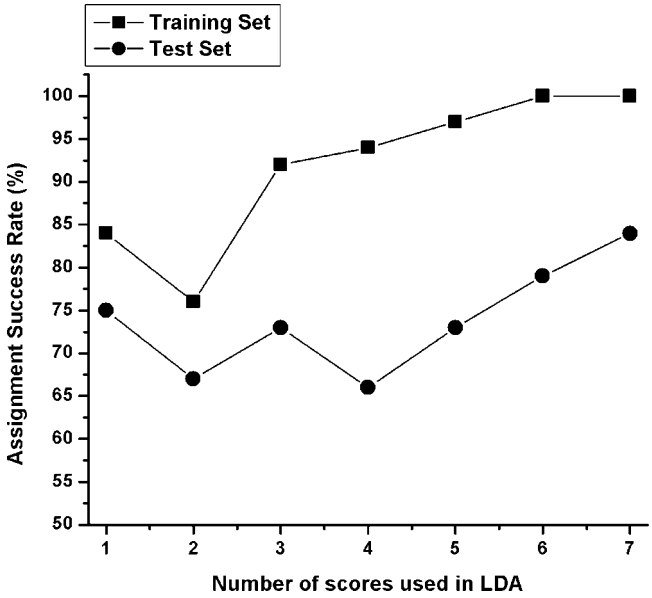


**Figure 20.** Reassignment and assignment success rates based on the number of PC scores used in LDA. Six PC scores were needed to assign 100% of the observations in the training set. 83% was the best achievable assignment rate for the test set.

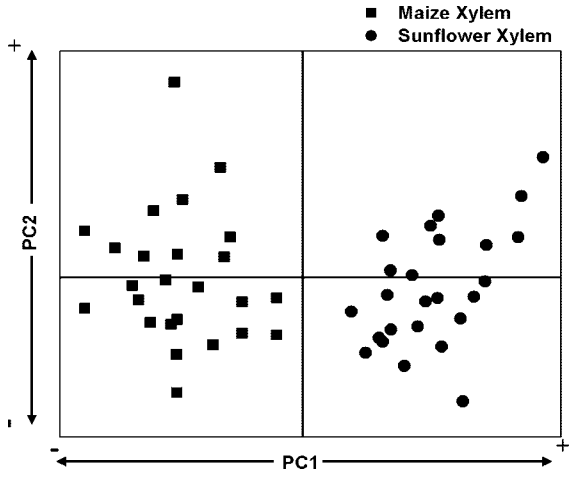


**Figure 21.** PCA score plot shows that maize and sunflower xylem can be separated by the first 2 PCs.

All of the samples from the maize test set were correctly assigned to the maize group. This shows that it is feasible to use PCA to distinguish between maize and sunflower epidermal tissue.

The dataset used to for the PCA of maize and sunflower cortex tissue consisted of 88 spectra, with 44 observations from each plant. The spectra were obtained and placed into the training and test sets using the same protocol described for the epidermal samples. A total of 32 cortex spectra from each plant were use to construct the training set. Parts **A** and **B** of **Figure 18** depict the PCA score plots generated using PCs 1 and 2 and PCs 3 and 5. The PCA plot using PC1 and PC2 shows that the samples were fairly dispersed, with no separation between the maize and sunflower samples. However, a plot of PC5 versus PC3 reveals some separation between the maize and sunflower samples. Even though the first and second PC loadings accounted for almost 85% of the overall variability, they were not able to separate the data into two distinct groups. The five PC loadings generated from PCA of the maize and sunflower cortex can be seen in **Figure 19**. The first PC loading (**Figure 19A**) shows positive peaks related to protein, with a shoulder

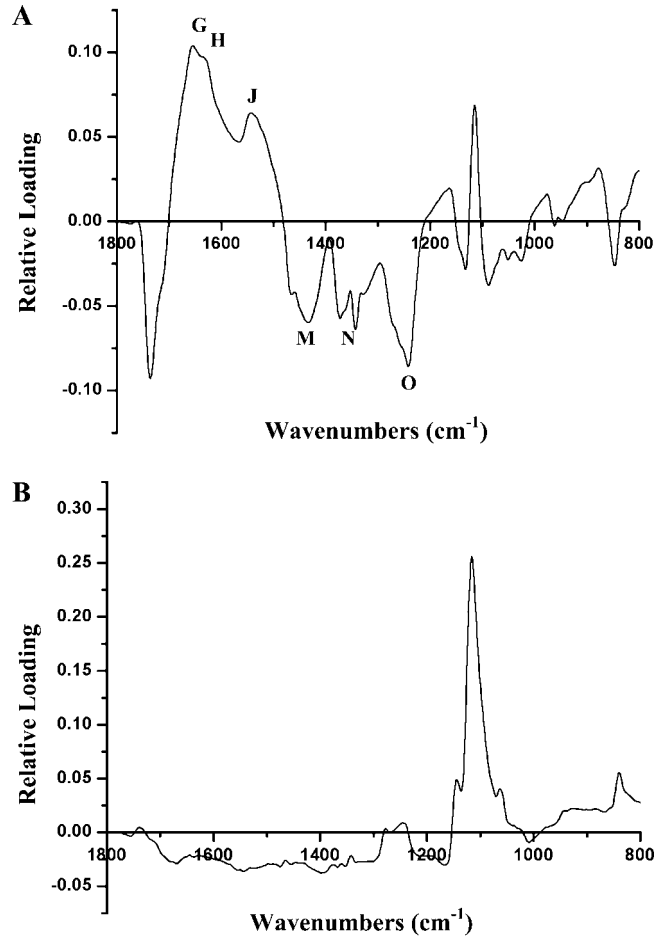


**Figure 22.** Loadings for the first (**A**) and second (**B**) PCs depicting the major variation between maize and sunflower xylem spectra. The first PC loading contains IR bands from all of the biopolymers. The second PC loading mostly contains peaks from the carbohydrate fingerprint region (band P). Refer to **Table 1** for a description of band assignments.

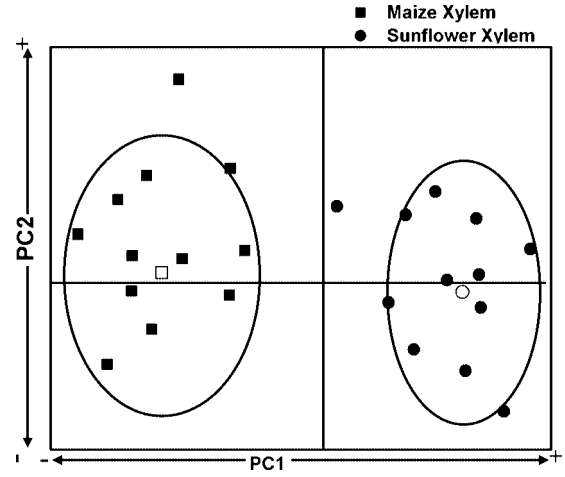


**Figure 23.** Validation plot used to test the robustness of the model set for maize and sunflower xylem. The hollow symbols represent the (□) maize and (○) sunflower group centers. The ovals represent the 95% tolerance regions. Two observations from each test set fell outside the 95% tolerance region and were not assigned to a group.

on the amide II peak (band G) representing C═O stretching of the carboxyl ester (band E). The second PC loading contains the amide I peak (band G) and peaks for polysaccharides and cellulose (band P). The third (**Figure 19C**) and fifth (**Figure 19E**) PC loadings account for 2.88 and 1.59% of the variability,

respectively. The constituents of the fifth PC loading are not noise but, in fact, are spectral bands associated with polysaccharides, protein, and cellulose. This loading, even though it contributes very little to the overall variability, represents some systematic variation between the maize and sunflower cortex. A total of 24 (12 for each plant) cortex spectra were taken from samples independent from the training set and used as the test set. Seven PC scores were used in the LDA, resulting in the correct assignment of 21 observations out of a total of 24 observations. The assignment and reassignment success rates based on the number of PC scores used in LDA are shown in **Figure 20**. In the training set, 6 PC scores were needed for a 100% success rate. The maximum success rate for the test set was 84%, meaning that the success rate did improve when increasing the PC scores as witnessed in the training set. This means that sunflower and maize cortex tissues are very similar and that infrared spectroscopy may not be sensitive enough to distinguish between them. Adding more independent samples to the training set may improve the ability to distinguish between maize and sunflower cortex tissue.

A total of 37 xylem spectra were extracted from 12 different maize samples, and 37 xylem spectra were obtained from 13 different sunflower samples using the same parameters mentioned for the comparison of sunflower and maize epidermal tissue. However, xylem spectra were sampled from maps of root tissue taken between 1 mm and 1 cm from the root tip. PCA was performed using 25 maize xylem spectra and 25 sunflower xylem spectra. The PCA score plot shown in **Figure 21** shows a clear separation of the maize and sunflower xylem samples using the first 2 PC scores, with the first PC providing the majority of the discrimination. The first PC score accounted for 71% of the variability, while the second PC score accounted for 16.5% of the variability, with an overall variability of 87.5%. The first PC loading (**Figure 22A**) indicates that maize xylem contains more protein (bands G and J) and sunflower xylem has more lipids (band E) and cellulose (band O). The second PC loading (**Figure 22B**) is somewhat similar to the second PC loading seen for the PCA of maize and sunflower epidermal tissue (**Figure 16B**). The positive peaks in the carbohydrate fingerprint region (band P) are representative of arabinogalactan as seen in maize epidermal tissue. The appearance of the IR peak at 1635 $cm^{-1}$ (band H), representing the presence of H-type lignin, is very significant because it also appeared in the PCA of epidermal tissue. In this study, the H-type lignin is unique to maize, thus providing a means of distinguishing maize from sunflower. A total of 24 xylem spectra taken from independent samples (12 for each plant) were used as the test set. Using the first two PC scores, 20 of 24 observations were correctly assigned to their appropriate group, as seen in the validation score plot in **Figure 23**. Two observations from each plant fell outside of the 95% confidence region, as expected. This is probably just a result of the natural variation within the plants themselves.

Because the IR bands for the common plant biopolymers were present in all of the IR spectra, it was clearly not possible to distinguish between maize and sunflower root tissue merely based on visual inspection of the IR spectra. This was especially true for samples from cortex or vascular tissue. The use of PCA allowed for the distinct separation of maize and sunflower samples using IR spectra from the epidermis and xylem. Even though it appeared that maize contained more protein and polysaccharides, such as arabinogalactan, these components were not sufficient to provide a distinction between maize and sunflower samples. The 1635 $cm^{-1}$ peak for hydrocinnamic acid in (H-type) lignin uncovered by PCA provided a conclusive means of distinguishing between maize and sunflower because of its uniqueness to maize, in this case. One could not distinguish between maize and another grass based on this parameter because H-type lignin is found in most monocots and all grasses. It is important to also note that this type of analysis is only semiquantitative. More independent samples are required for the training set to provide a more reliable means to quantify the biopolymers present in the maize and sunflower samples. However, these findings do suggest that infrared imaging in conjunction with PCA can become an effective means to analyze plant structure and development. With the ready availability of focal plane array (FPA) detectors, comparable spectral analysis can be perfromed in a similar time frame with a globar source. If signal-to-noise is not a major consideration, the FPA systems may be somewhat faster. In this case, although, the resolution will not be diffraction-limited but pixel-dimension-limited, a restriction that is more important at higher wavenumbers, e.g., 2000−5000 $cm^{-1}$ (*35*).

## ACKNOWLEDGMENT

The authors thank Nebojsa Marinkovic for his assistance on beamline U2B at the NSLS at BNL and the Kansas State University Veterinary Diagnostic Laboratory, supervised by Cindy Chard-Bergstrom, for the use of their cryomicrotome.

## LITERATURE CITED

(1) Carpita, N. C.; McCann, M. C. The functions of cell wall polysaccharides in composition and architecture revealed through mutations. *Plant Soil* **2002**, *247*, 71–80.

(2) Carpita, N. C.; Defernez, M.; Findlay, K.; Wells, B.; Shoue, D. A.; Catchpole, G.; Wilson, R. H.; McCann, M. C. Cell wall architecture of the elongating maize coleoptile. *Plant Physiol.* **2001**, *127*, 551–565.

(3) Jarvis, M. C.; McCann, M. C. Macromolecular biophysics of the plant cell wall: Concepts and methodology. *Plant Physiol. Biochem.* **2000**, *38*, 1–13.

(4) Dokken, K. M.; Davis, L. C.; Marinkovic, N. S. Use of infrared spectroscopy in plant growth and development. *Appl. Spectrosc. Rev.* **2005**, *40*, 301–326.

(5) Wetzel, D. L.; Srivarin, P.; Finney, J. R. Revealing protein infrared spectral detail in a heterogeneous matrix dominated by starch. *Vib. Spectrosc.* **2003**, *31*, 109–114.

(6) Wetzel, D. L.; LeVine, S. M. Biological applications of infrared microspectrocscopy. In *Infrared and Raman Spectroscopy of Biological Materials*; Gremlich, H.-U., Yan, B., Eds.; Marcel Dekker: New York, 2001; pp 101–142.

(7) Wetzel, D. L.; Eilert, A. J.; Pietrzak, L. N.; Miller, S. S.; Sweat, J. A. Ultraspatiallyresolved synchrotron infrared microspectroscopy of a plant tissue in situ. *Cell. Mol. Biol.* **1998**, *44*, 145–167.

(8) Yu, P. Applications of advanced synchrotron radiation-based Fourier transform infrared (SR−FTIR) microspectroscopy to animal nutrition and feed science: A novel approach. *Br. J. Nutr.* **2004**, *92*, 869–885.

(9) Yu, P.; McKinnon, J. J.; Christensen, C. R.; Christensen, D. A. Using synchrotron-based FTIR microspectroscopy to reveal chemical features of feather protein secondary structure: Comparison with other feed protein sources. *J. Agric. Food Chem.* **2004**, *52*, 7353–7361.

(10) Yu, P. Application of cluster analysis (CLA) in feed chemical imaging to accurately reveal structural−chemical features of feed and plants within cellular dimension. *J. Agric. Food Chem.* **2005**, *53*, 2872–2880.

(11) Yu, P.; McKinnon, J. J.; Christensen, C. R.; Christensen, D. A. Imaging molecular chemistry of Pioneer corn. *J. Agric. Food Chem.* **2004**, *52*, 7345–7352.

(12) Yu, P.; Christensen, D. A.; Christensen, C. R.; Drew, M. D.; Rossnagel, B. G.; McKinnon, J. J. Use of synchrotron FTIR microspectroscopy to identify chemical differences in barley endosperm tissue in relation to rumen degradation characteristics. *Can. J. Anim. Sci.* **2004**, *84*, 523–527.

(13) Yu, P.; McKinnon, J. J.; Christensen, C. R.; Christensen, D. R. Using synchrotron transmission FTIR microspectroscopy as rapid, direct,and nondestructive analytical technique to reveal molecular microstructural−chemical features within tissue in grain barley. *J. Agric. Food Chem.* **2004**, *52*, 1484–1494.

(14) Yu, P.; McKinnon, J. J.; Christensen, C. R.; Christensen, D. R.; Marinkovic, N. S.; Miller, L. M. Chemical imaging of microstructures of plant tissues within cellular dimension using synchrotron infrared microspectroscopy. *J. Agric. Food Chem.* **2003**, *51*, 6062–6067.

(15) Yu, P.; Christensen, C. R.; Christensen, D. A.; McKinnon, J. J. Ultrastructural−chemical makeup of yellow-seeded (*Brassica rapa*) and brown-seeded (*Brassica napus*) canola within cellular dimensions, explored with synchrotron reflection FTIR microspectroscopy. *Can. J. Plant Sci.* **2005**, *85*, 533–541.

(16) Dokken, K. M.; Davis, L. C.; Erickson, L. E.; Castro-Diaz, S.; Marinkovic, N. S. Synchrotron Fourier transform infrared microspectroscopy: A new tool to monitor the fate of organic contaminants in plants. *Microchem. J.* **2005**, *81*, 86–91.

(17) Dokken, K. M.; Davis, L. C.; Marinkovic, N. S. Synchrotron radiation infrared microspectroscopy (SR−IMS) as a tool to study the fate and transport of organic contaminants in plants. *Spectroscopy* **2005**, *20*, 14–20.

(18) Raab, T. K.; Martin, M. C. Visualizing rhizosphere chemistry of legumes with mid-infrared synchrotron radiation. *Planta* **2001**, *213*, 881–887.

(19) Raab, T. K.; Vogel, J. P. Ecological and agricultural applications of synchrotron microscopy. *Infrared Phys. Technol.* **2004**, *24*, 393–402.

(20) Séné, C. F. B.; McCann, M. C.; Wilson, R. H.; Grinter, R. Fourier-transform Raman and Fourier-transform infrared spectroscopy: An investigation of five higher plant cell walls and their components. *Plant Physiol.* **1994**, *106*, 623–1631.

(21) McCann, M. C.; Chen, L.; Roberts, K.; Kemsley, E. K.; Sene, C.; Carpita, N. C.; Stacey, N. J.; Wilson, R. H. Infrared microspectroscopy: Sampling heterogeneity in plant cell wall composition and architecture. *Physiol. Plant.* **1997**, *100*, 729–738.

(22) Castro, S.; Davis, L. C.; Erickson, L. E. Temperature and pH effects on plant uptake of benzotriazoles by sunflowers in hydroponic culture. *Int. J. Phytorem.* **2004**, *6*, 209–225.

(23) Kemsley, E. K. *Discriminant Analysis and Class Modelling of Spectroscopic Data*; John Wiley and Sons: Chichester, U.K., 1998.

(24) Sutherland, G. B. B. M. Infrared analysis of amino acids, polypeptides and proteins. *Biochim. Biophys. Acta* **1952**, *6*, 291–318.

(25) Williams, D. H.; Fleming, I. Infrared Spectroscopy. In *Spectroscopic Methods in Organic Chemistry*; McGraw-Hill: New York, 1980; pp 35–73.

(26) Hergert, H. L. Infrared spectra. In *Lignins: Occurrence, Formation, Structure, and Reactions*; Sarkanen, K. V., Ludwig, C. H., Eds.; John Wiley and Sons: New York, 1971; pp 267–297.

(27) Kacurakova, M.; Capek, P.; Sasinkova, V.; Wellner, N.; Ebringerova, A. FT-IR study of plant cell wall model compounds: Pectic polysaccharides and hemicelluloses. *Carbohydr. Polym.* **2000**, *43*, 195–203.

(28) Zeier, J.; Schreiber, L. Fourier transform infrared-spectroscopic characterization of isolated endodermal cell walls from plant roots: Chemical nature in relation to anatomical development. *Planta* **1999**, *209*, 537–542.

(29) Vicre, M.; Santaella, C.; Blanchet, S.; Gateau, A.; Driouich, A. Root border-like cells of *Arabidopsis*. Microscopical characterization and the role in the interaction with rhizobacteria. *Plant Physiol.* **2005**, *138*, 998–1008.

(30) Aspinall, G. O. Chemistry of cell wall polysaccharides. In *The Biochemistry of Plants, Volume 3 Carbohydrates: Structure and Function*; Preiss, J., Ed.; Academic Press: New York, 1980; pp 473–500.

(31) Carpita, N. C. Structure and biogenesis of the cell walls of grasses. *Ann. Rev. Plant Physiol. Plant Mol. Biol.* **1996**, *47*, 445–476.

(32) Fry, S. C. Feruloylated pectins from the primary cell wall: Their structure and possible functions. *Planta* **1983**, *157*, 111–23.

(33) Gibeaut, D. M.; Carpita, N. C. Tracing cell wall biogenesis in intact cells and plants: Selective turnover and alteration of soluble and cell wall polysaccharides in grasses. *Plant Physiol.* **1991**, *97*, 551–561.

(34) Hose, E.; Clarkson, D. T.; Steudle, E.; Schreiber, L.; Hartung, W. The exodermis: A variable apoplastic barrier. *J. Exp. Bot.* **2001**, *52*, 2245–2264.

(35) Zeier, J.; Schreiber, L. Chemical composition of hypodermal and endodermal cell walls and xylem vessels isolated from *Clivia miniata*. *Plant Physiol.* **1997**, *113*, 1223–1231.

**Received for review July 9, 2007. Revised manuscript received October 29, 2007. Accepted November 1, 2007. Funding for experimentation at the National Synchrotron Light Source (NSLS) at Brookhaven National Laboratory (BNL) was provided by the U.S. Department of Energy (DOE). Further support was provided by the United States Environmental Protection Agency (USEPA) under assistance agreement R-825550 through the Great Plains/Rocky Mountain Hazardous Substance Research Center and the Kansas Agricultural Experiment Station, contribution 07-303-J.**

JF072052E